SSS ELSEVIER

Contents lists available at ScienceDirect

Science of the Total Environment

journal homepage: www.elsevier.com/locate/scitotenv



Refining real-time predictions of *Vibrio vulnificus* concentrations in a tropical urban estuary by incorporating dissolved organic matter dynamics



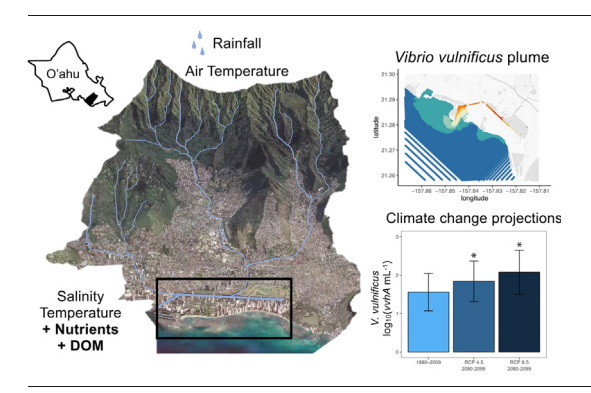
Jessica A. Bullington ^{a,b,c,*}, Abigail R. Golder ^{b,d}, Grieg F. Steward ^{a,b}, Margaret A. McManus ^a, Anna B. Neuheimer ^{a,e}, Brian T. Glazer ^a, Olivia D. Nigro ^f, Craig E. Nelson ^{a,b,c}

- ^a Department of Oceanography, University of Hawaiʻi at Mānoa, Honolulu, HI, United States
- b Daniel K. Inouye Center for Microbial Oceanography: Research and Education (C-MORE), Honolulu, HI, United States
- ^c Sea Grant College Program, University of Hawaiʻi at Mānoa, Honolulu, HI, United States
- d Department of Biological Sciences, Virginia Institute of Marine Science, Gloucester Point, VA, United States
- ^e Department of Biology, Aarhus University, Aarhus, Denmark
- f Department of Natural Science, Hawai'i Pacific University, Honolulu, HI, United States

HIGHLIGHTS

- Habitat range and incidence of infections by *V. vulnificus* are increasing.
- Models to predict coastal water concentrations of *V. vulnificus* were evaluated.
- In situ sensor data and physical models can inform pathogen risk assessment.
- Rain events transport and elevate concentrations of *V. vulnificus* on the coast.
- V. vulnificus abundance is projected to increase in coastal waters of Hawai'i.

GRAPHICAL ABSTRACT



ARTICLE INFO

Article history: Received 15 August 2021 Received in revised form 14 January 2022 Accepted 17 February 2022 Available online 24 February 2022

Editor: Ashantha Goonetilleke

Keywords:
Vibrio vulnificus
Pathogen
Hawai'i
Dissolved organic matter
Predictive modeling
Climate change

ABSTRACT

The south shore of Oʻahu, Hawaiʻi is one of the most visited coastal tourism areas in the United States with some of the highest instances of recreational waterborne disease. A population of the pathogenic bacterium *Vibrio vulnificus* lives in the estuarine Ala Wai Canal in Honolulu which surrounds the heavily populated tourism center of Waikiki. We developed a statistical model to predict *V. vulnificus* dynamics in this system using environmental measurements from moored oceanographic and atmospheric sensors in real time. During a year-long investigation, we analyzed water from 9 sampling events at 3 depths and 8 sites along the canal (n = 213) for 36 biogeochemical variables and *V. vulnificus* concentration using quantitative polymerase chain reaction (qPCR) of the hemolysin A gene (*vvhA*). The best multiple linear regression model of *V. vulnificus* concentration, explaining 80% of variation, included only six predictors: 5-day average rainfall preceding water sampling, daily maximum air temperature, water temperature, nitrate plus nitrite, and two metrics of humic dissolved organic matter (DOM). We show how real-time predictions of *V. vulnificus* concentration can be made using these models applied to the time series of water quality measurements from the Pacific Islands Ocean Observing System (PacIOOS) as well as the PacIOOS plume model based on the Waikiki Regional Ocean Modeling System (ROMS) products. These applications highlight the importance of including DOM variables in predictive modeling of *V. vulnificus* and the influence of rain events in elevating nearshore concentrations of *V. vulnificus*. Long-term climate model projections of locally downscaled monthly rainfall and air temperature were

Corresponding author.
 E-mail address: jbulling@hawaii.edu (J.A. Bullington).

used to predict an overall increase in *V. vulnificus* concentration of approximately 2- to 3-fold by 2100. Improving these predictive models of microbial populations is critical for management of waterborne pathogen risk exposure, particularly in the wake of a changing global climate.

1. Introduction

Vibrio is a genus of Gram-negative heterotrophic bacteria with diverse life history strategies as free-living, host-associated, or particle-attached members of marine and estuarine microbial communities worldwide (Baker-Austin et al., 2018; Heng et al., 2017; Huang et al., 2016). Several Vibrio species are known human pathogens, including V. cholerae, V. parahaemolyticus, and V. vulnificus. Vibrio infections occur as a result of foodborne or environmental exposure with an annual healthcare cost to the U.S. nearing \$300 million with approximately 85% of those costs attributed to V. vulnificus alone (Ralston et al., 2011). Although reported human infections caused by V. vulnificus are infrequent (~100 cases reported in the U.S. annually), the hospitalization rate associated with those cases is over 80% (Newton et al., 2012). In cases identified as primary septicemia, the fatality rate is over 50% (Horseman and Surani, 2011; Jones and Oliver, 2009). Unlike sewage-borne human pathogens, V. vulnificus concentrations cannot be predicted using fecal indicator bacteria. This pathogen lives naturally in estuarine habitats (Strom and Paranjpye, 2000). V. vulnificus is found both free-living in brackish water and associated with sediment, algae, fish, molluscs, crustaceans, and zooplankton in warm estuarine environments globally (DePaola et al., 1994; Givens et al., 2014; Johnson et al., 2010; Maugeri et al., 2006; Turner et al., 2009). There is minimal monitoring for V. vulnificus in coastal waters worldwide (Baker-Austin et al., 2018), particularly at relevant spatial scales that would allow for reliable forecasting. Predicting the presence and abundance of V. vulnificus will become even more critical with climate change. Increasing water temperatures and rising sea levels are likely to promote the pathogen's growth and habitat expansion (Froelich and Daines, 2020).

Estuaries are heterogeneous and idiosyncratic with unique biogeochemical features and high biological diversity and activity (Cai, 2011). They are known to be effective traps for nutrients, sediments, and pollutants from inflowing rivers and runoff (Shiller, 1996). By nature of their proximity to populous areas, estuaries are at high risk of anthropogenic impact from development and pollution. Due to complex and location-specific hydrology, oceanography, climatology, and human development, it is unknown how climate change will modify these environments, particularly estuarine microbial communities and the abundance of human pathogens (Ghosh and Bhadury, 2019; Kan et al., 2007).

There is empirical evidence of increasing abundances of V. vulnificus in coastal waters and increasing V. vulnificus infection rates over the past 50 years (Newton et al., 2012) which have been linked to increased sea surface temperature (Vezzulli et al., 2012, 2013, 2016). Additional climatological changes, such as increased frequency of hurricanes, storm surges, sea level rise, and coastal flooding, have been hypothesized to spread the distribution of V. vulnificus to upland watersheds and increase the incidence of V. vulnificus infections (Martinez-Urtaza et al., 2010; Muhling et al., 2017; Paz et al., 2007). Muhling et al. (2017) found significant expansion of the spatial and seasonal occurrences of V. vulnificus in the Chesapeake Bay based on statistical downscaling of climate change projections. There is evidence for habitat expansion into higher latitudes (Baker-Austin et al., 2013; Paz et al., 2007) and a decrease of V. vulnificus abundance during drought conditions (Wetz et al., 2013). Although the risks of V. vulnificus infection from recreational exposure appear to be increasing, environmental monitoring of V. vulnificus abundance in seawater is not routine in the U.S. Predictive models (based on the environmental conditions that govern V. vulnificus distribution and growth) may be a practical alternative to laborious survey-based monitoring and provide an early warning of the risk of infection. Previous work has shown promise at constructing spatiallyexplicit predictive models. However, these efforts have been limited to probability of occurrence (Banakar et al., 2011) and high versus low

abundance (Jacobs et al., 2014) rather than absolute abundance of *V. vulnificus* which is more directly related to the risk of exposure.

The environmental controls of V. vulnificus populations are poorly constrained aside from the well-established effects of salinity and temperature on growth rates in laboratory cultures (Kaspar and Tamplin, 1993; Motes et al., 1998) and on abundance in situ (Lipp et al., 2001; Nigro and Steward, 2015; O'Neill et al., 1992; Randa et al., 2004; Tamplin et al., 1982; Wright et al., 1996). There is general consensus that V. vulnificus is most prolific in water temperatures above 18 °C and salinities between 15 and 25. There are only a few field-based studies that assess the effects of additional environmental conditions, such as turbidity and nutrients (Pfeffer et al., 2003). In situ measurements of V. vulnificus density show strong seasonal dynamics where V. vulnificus density is higher in warm summer months in temperate and subtropical areas (Huehn et al., 2014; Jacobs et al., 2014; Pfeffer et al., 2003; Tamplin et al., 1982). However, there is minimal data from tropical areas (Nigro et al., 2022; Rivera et al., 1989) where water temperatures remain above 18 °C year-round and other environmental controls may be more important determinants of V. vulnificus density.

Tropical coastal waters, with year-round warm temperatures, might be expected to have persistently high Vibrio spp. concentrations, and thus relatively high rates of reported infections. The incidence of non-cholera Vibrio infections reported to the Centers for Disease Control and Prevention (https://www.cdc.gov/vibrio/surveillance.html) is in fact higher for Hawai'i (20-40 cases per year per capita) than any other U.S. state. Despite this relative high risk of vibriosis infections resulting from recreational water exposure in Hawai'i, there have been comparatively few studies of Vibrio spp. in coastal waters in Hawai'i (Viau et al., 2011; Vithanage, 2011). A fatal V. vulnificus infection contracted by an individual who had open wounds exposed to waters of the Ala Wai Harbor on O'ahu, HI (Antone, 2006) motivated a detailed investigation into the spatial and temporal varability of V. vulnificus in the harbor and the Ala Wai Canal that drains into it over the course of a year from 2008 to 2009 (Nigro et al., 2022). This sampling was conducted in a nested design: monthly for one year, weekly for July and March, daily for one week in July and March, and hourly for one day in July. In that study, temperature explained little of the variability in V. vulnificus abundance. Instead, V. vulnificus had a significant, but non-linear relationship with salinity in the canal, with higher abundances on average in the rainier winter months compared to the drier summer. The authors suggested that this creates a tendency toward a rainfall-driven seasonal cycle in Hawai'i that is inverted from the temperature-driven cycle seen in temperate waters. The pattern is expected to be highly variable, however, because of the stochasticity in rainfall and the suppressive effects of both very low and very high rainfall (Nigro et al., 2022). These data were used in previous modeling attempts in this system using a coupled physical circulation and numerical model of V. vulnificus growth rate in response to salinity and temperature by Nuss (2016). However, there were significant discrepancies between modeled and measured V. vulnificus abundance warranting further exploration for statistical and predictive modeling.

In this study, we have conducted a second year-long investigation of *V. vulnificus* in the Ala Wai Canal and Harbor a decade after the prior study, expanding it to include sampling at multiple depths, sites outside the harbor, and measurement of many additional environmental variables. Statistical models for predicting *V. vulnificus* abundance derived from these data were combined with an existing turbidity plume forecast model (Johnson et al., 2013) maintained by the Pacific Islands Ocean Observing System (PacIOOS) to construct a real-time model of *V. vulnificus* density throughout nearshore Waikīkī. We envision that this model will provide more timely information on pathogen risk assessment. In addition, we

report a long-term forecast of V. vulnificus densities with local climate change projections.

2. Materials and methods

2.1. The Ala Wai Canal study site

The Ala Wai Canal is a prominent waterway in urban Honolulu, Hawai'i on the island of O'ahu. The canal was constructed during the 1920s by the U.S. Army Corps of Engineers to drain the Waikīkī wetlands for coastal development. The canal is channelized with concrete and extends for roughly 3 km parallel to the shoreline varying from 51 to 83 m wide with one major bend toward the ocean. Currently, the canal operates as a tidally-influenced estuary with freshwater input from the Makiki stream, Mānoa-Pālolo drainage, and several small urban runoff drains. The mouth of the canal is located at the Ala Wai Boat Harbor centered between the popular Waikīkī beaches to the east and Ala Moana Beach Park to the west. In this potential outflow area, there is high recreational activity, including surfing, paddling, sailing, swimming, and fishing. There are canoe clubs located along the canal and paddlers that traverse the canal itself. Therefore, there is a concerning risk of exposure to V. vulnificus in this area. The Clean Water Branch (CWB) of the Hawai'i State Department of Health is responsible for the protection and monitoring of the coastal ecosystem in the state. The CWB tests coastal waters for fecal indicator bacteria concentrations (Enterococcus spp. and Clostridium perfringens), as well as water chemistry (pH, salinity, DO, turbidity, and temperature) (http://cwb.doh.hawaii. gov/CleanWaterBranch/WaterQualityData/default.aspx). However, the CWB sampling in the Ala Wai Canal has been suspended due to budgetary constraints and V. vulnificus is not routinely monitored by the CWB anywhere in Hawai'i. Previous studies investigating rain-driven effluent plumes from the canal suggest that the canal could be a source of pathogenic bacteria into coastal waters (Connolly et al., 1999; Johnson et al., 2013). V. vulnificus is also prevalent throughout the canal and its abundance was observed to vary in response to rates of freshwater input from surface runoff and groundwater (Nigro et al., 2022).

2.2. Field surveys and sample collection

Biogeochemical survey data were collected over 9 sampling dates between October 2018 and October 2019 (21 October 2018; 29 November 2018; 20 January 2019; 18 February 2019; 22 March 2019; 20 April 2019; 4 June 2019; 31 August 2019; 29 September 2019). Depth profiles were collected from 18 sites along the Ala Wai Canal and offshore (Fig. 1). Sites located in the harbor and offshore regions are areas of high recreational use. Continuous sensor profiles were conducted at each site on each date for salinity, temperature, turbidity, chlorophyll fluorescence, and dissolved oxygen. Discrete bottle samples (n = 213 total; one sample per site and depth for each month) were collected at 8 of these sites roughly 0.5 km apart along the transect. For discrete sampling, water was pumped into 1 L polycarbonate bottles at 3 depths per site: surface (25 cm below the air-water interface), middle (targeting the pycnocline which ranged from 0.34-5.09 m depth), and bottom (25 cm above the sediment-water interface which ranged from 0.52-11.59 m depth). Sampling was conducted sequentially along the sites and against the tidal flow over a period of \sim 3 h. We targeted sampling from the back of the canal at the lowest low tide for consistency and maximal gradient in salinity. Bottle samples were processed or preserved within 8 h of collection.

2.3. Hydrological and climatological data sources

For each sampling date, Mānoa stream water height and discharge data were downloaded from the United States Geological Survey (USGS) National Water Information System (https://waterdata.usgs.gov/HI/nwis/current/?type=dailydischarge&group_key=basin_cd) for site 16240500 (21.328222°N, $-157.799611^\circ E$). Tide data were downloaded from the National Oceanic and Atmospheric Administration (NOAA) Tides and

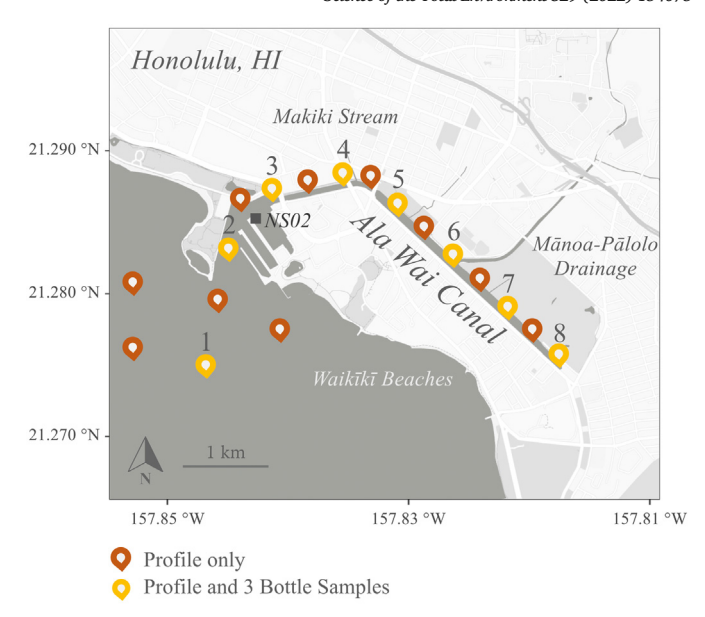


Fig. 1. Map of the Ala Wai Canal in Honolulu, Hawaiʻi depicting monthly survey sampling locations from October 2018–September 2019. Full depth profiles for salinity, temperature, dissolved oxygen, turbidity, and chlorophyll were collected from all sites (n=18) marked with a pin. Numbered sites (1-8) are locations where discrete bottle samples were collected at 3 depths (surface, pycnocline, and bottom water) for additional nutrient, organic matter, and microbial measurements. The PacIOOS nearshore sensor NS02 at the Ala Wai Harbor is marked with a grey box.

Currents (https://tidesandcurrents.noaa.gov/datums.html?id=1612340) for site 1612340 (21.306667°N, - 157.866667°E). Air temperature and precipitation data were downloaded from the NOAA National Centers for Environmental Information (https://www.ncdc.noaa.gov/cdo-web/search) Global Historical Climatology Network for site GHCND: USW00022521 (21.324°N, -157.9294°E) and GHCND:USC00516122 (21.3113°N, -157.8157°E), respectively.

2.4. Water chemistry data collection

2.4.1. In situ sensor data collection

Temperature and conductivity were measured using an Aanderaa 4319A conductivity sensor (1.4 Hz). Dissolved oxygen was measured using an Aanderaa 4330F optode (~ 1 Hz). Turbidity (approximated from optical backscatter) and chlorophyll-a fluorescence were measured using a Sea-Bird ECO FLNTU sensor (~ 6 Hz). Depth was measured using a custom-built water pressure probe (~ 1 Hz). Precise latitude and longitude were recorded using an onboard Simrad GPS.

2.4.2. Nutrient measurements

All nutrient samples were analyzed at the University of Hawai'i at Mānoa School of Ocean and Earth Science and Technology (SOEST) Laboratory for Analytical Biochemistry (http://www.soest.hawaii.edu/S-LAB/) using a Seal Analytical AA3 HR Nutrient Autoanalyzer. Dissolved nitrate plus nitrite, ammonium, phosphate, and silicate were analyzed according to Armstrong et al. (1967) and Grasshoff et al. (1983), Kérouel and Aminot (1997), Murphy and Riley (1962), and Grasshoff et al. (1983), respectively, following filtration through a 0.22 μm pore size polyethersulfone filter capsule (Sterivex, Millipore) using a peristaltic pump. Total nitrogen and total phosphorus were measured from non-filtered samples following the modified Autoanalyzer procedure developed by the University of Hamburg.

2.4.3. Particulate and dissolved organics measurements

Particulate organic carbon (POC) and particulate organic nitrogen (PON) samples were collected on combusted GF/F filters (Whatman) and

analyzed using an Exeter Analytical model 440 CE elemental analyzer according to methods by Gordon (1969) and Sharp (1974). Filtrate was collected and acidified to pH 2 to measure dissolved organic carbon (DOC) and total dissolved nitrogen (TDN) using a Shimadzu High-Temperature TOC-L Combustion Analyzer. Samples for fluorescent dissolved organic matter (fDOM) were analyzed using a Horiba Aqualog scanning fluorometer according to Nelson et al. (2015). Relative fluorescence of known spectral peaks in excitation emission matrices was determined based on Coble (1996).

2.4.4. pH measurements

Measurements of pH were made from whole water bottle samples in the lab using a Hach sensor probe calibrated for each sampling event.

2.5. Microbial data collection

2.5.1. Chlorophyll-a measurements

Chlorophyll-a was measured from bottle samples using acetone extraction from material collected on 0.45 μm HAWP filters (Millipore) and fluorescence spectroscopy on a modified Turner 10 AU fluorometer according to Smith et al. (1981) with a detection limit of 0.025 $\mu g~L^{-1}$ using the EPA Method 445.0.

2.5.2. Total prokaryotic abundance measurements

Total prokaryotic abundance was determined using an Attune Acoustic Focusing Cytometer according to Nelson et al. (2015) from whole water samples fixed with paraformaldehyde (0.5% final concentration) and stained with $1\times$ SYBR Green I.

2.5.3. DNA extraction protocol

Samples for DNA extraction (n=213) were collected by passing water through 0.22 µm polyethersulfone filters (Sterivex, Millipore); the exact filtrate volume was recorded (250–500 mL). This volume was sufficient for DNA extraction yield and qPCR detection. Filter housings were cracked open with pliers and filters were removed with a sterile razor blade and added to MP Biomedicals Lysing Matrix A (No. 116910100) tubes with 0.5 mL MC 1 lysis buffer and homogenized using a MP Biomedicals FastPrep-96 bead beater. A portion of the homogenate (0.4 mL) was recovered and DNA extractions were completed using the Macherey-Nagel NucleoMag Plant Extraction Kit (No. 744400.4) with KingFisher Accessory Kit (No. 744951). Samples were eluted to a final volume of 110 µL.

2.5.4. Quantifying Vibrio vulnificus

There is a consistent log correlation between CHROMagar Vibrio blue colony forming units and V. vulnificus hemolysin A (vvhA) gene copy concentrations (Nigro and Steward, 2015). Therefore, we used a 5' nuclease vvhA quantitative PCR assay (Campbell and Wright, 2003; Holland et al., 1991; forward primer: 5'-TGTTTATGGTGAGAACGGTGACA-3'; reverse primer: 5'-TTCTTTATCTAGGCCCCAAACTTG-3'; 5'-nuclease probe: 5'-/ 56-FAM/CCGTTAACC/ZEN/GAACCACCCGCAA/31ABkFQ/-3') to determine total V. vulnificus abundance. A 25 μ L reaction mixture was prepared with final concentrations of 1× Kapa Probe Force Master Mix (Kapa Biosystems), 0.9 μM of each primer, 0.5 μM of the labeled probe, 0.56 mg/mL bovine serum albumin (Thermo Fisher Scientific), and 5 μ L of DNA template (11.4-22.7 mL sample water). All qPCR reactions were performed in triplicate from each biological sample (n = 213) with the final technical replicate diluted 10-fold to check for inhibition of amplification as suggested by Bustin et al. (2009). The cycling protocol consisted of an initial denaturation step at 95 °C for 10 min, followed by 40 cycles of denaturation at 95 °C for 15 s and a combined annealing/extension at 60 °C for 30 s. We created an eight-point standard curve (10-50,000 copies per reaction well) of genomic DNA from V. vulnificus (strain YJ016; Chen et al., 2003) with known gene copy numbers per reaction run in triplicate along with the environmental samples. Assay efficiency was calculated from multiple standard curves using the formula $E = -1 + 10^{(-1/\text{slope})}$ (Pfaffl, 2001). Samples were re-analyzed or removed from the data set if the

qPCR assay was inhibited (diluted replicate was greater than 10 times the average of the other replicates) or if the diluted replicate was not detected. If no replicates were detected after multiple assays, the sample was set to the lowest detectable copy number (0.1 νvhA gene copies mL $^{-1}$ sample water).

2.6. Data analysis

2.6.1. Data availability

Data and analysis code are available through the GitHub repository (https://github.com/jessicabullington/AlaWai-vvhA-2018-2019) (Bullington, 2022).

2.6.2. Data processing

Data collected from sensors (salinity, temperature, dissolved oxygen, chlorophyll, and turbidity) were resampled to 1 Hz frequency with linear interpolation using Python 3.7.4 (Python Core Team, 2015) pandas package (McKinney, 2011) in order to coordinate the datasets based on timestamp. These data were then averaged over the time the bottle sample was collected to combine with discrete bottle measurements (nutrients, organics, pH, chlorophyll-a, total prokaryotes, *vvhA*). Replicate qPCR measurements of *vvhA* gene copy number were averaged and those below the assay limit of detection (10 copies per reaction) were set to the lowest detectable measurement of 0.1 copies mL⁻¹ sample volume. *V. vulnificus* concentration (*vvhA* gene copies mL⁻¹) were log₁₀-transformed.

2.6.3. Statistical analysis and model selection

We hypothesized that spatial and temporal variation in environmental and climatological variables could explain significant variation in V. vulnificus density. In particular, we hypothesized that including characterization of DOM significantly improves previous statistical models of V. vulnificus density in the Ala Wai Canal and Harbor. We also hypothesized that the resolution of vertical structure of biogeochemical predictors would improve coupling to the physical circulation model. To avoid collinearity between model predictors, we assessed pairwise correlation of all predictors in a correlation matrix. A hierarchical cluster based on the correlation matrix was generated and one or two predictors were chosen from each major cluster (Suppl. Fig. 1) to be included in the full model for further analysis. To maximize the usefulness of the final model, we prioritized parameters that are widely measured, lower cost, and available on continuous monitoring platforms. We used multiple linear regression analyses to test our hypotheses. While there are more sophisticated modeling techniques, such as artificial neural networks, we chose to use more simplistic linear regression models which are easy to interpret and implement by managers of this system and other tropical estuaries globally.

We fit a linear model of log₁₀-transformed V. vulnificus density (the response variable) with an error distribution assumption of normal. The model included main effects of predictors only with no interaction terms in order to maximize ease of usability in other systems. Multicollinearity of predictors in the full model was further assessed with variance inflation factors (VIF) and predictors above 5 were removed. Model assumptions were assessed by inspection of residuals for normality and uniformity. When necessary, data were transformed, typically with log₁₀, to improve residual error distributions. Linear regression analyses were performed using R version 3.1.6 (R Core Team, 2019). The best combination of predictors was determined by fitting all possible predictor combinations using the dredge function in the MuMIn package (Bartoń, 2019) and comparing the Akaike Information Criterion value (Akaike, 1973) corrected for small samples sizes (AICc). The importance of each predictor was evaluated using the importance function from the MuMIn package. The importance value is the sum of the model Akaike weights for all models that contain the particular parameter. Leave-one-out cross-validation was used to evaluate prediction error (PE). One observation was set aside for validation and the remaining observations (99% in this case) were used to train the model and the process was repeated for each observation. The root mean squared error

(RMSE), the average difference between predictions and observations, was then \log_{10} -corrected to determine the PE.

2.6.4. Short-term forecasting

Short-term forecasting, or nowcasting, of V. vulnificus density was developed using the PacIOOS nearshore sensor NS02 (http://www.pacioos. hawaii.edu/water/sensor-hawaiiyachtclub/) and the PacIOOS turbidity plume forecast (http://www.pacioos.hawaii.edu/water/model-plumealawai/) based on the Regional Ocean Modeling System for the Waikīkī area (Waikīkī ROMS). The PacIOOS NS02 is moored at 1 m depth at (21.286407°N, -157.84276°E) and records continuous measurements of temperature and conductivity (Sea-Bird Electronics, SBE16plus V2 SEACAT), and fluorescence (470/695 nm) from which chlorophyll-a is estimated, and optical backscatter (700 nm) as an approximation of turbidity (WET Labs, ECO FLNTUS) at 0.0042 Hz frequency (McManus, 2008). An additional sensor for continuous measurements of fDOM (WET Labs, WETStar DOM Fluorometer, 370 nm excitation/460 nm emission, 0.0014 Hz; Belzile et al., 2006) was deployed at this location from September 2018 - May 2019. These measurements were validated based on depth profile measurements in this study at site 2. V. vulnificus density was predicted using PacIOOS NS02 salinity and water temperature plus the NOAA National Weather Service (NWS) five-day average rainfall and daily maximum air temperature. Predictions were compared to measured V. vulnificus density. A second model of V. vulnificus density which included fDOM measurements was compared to the previous model to assess the effect of adding DOM as a model parameter. Goodness of fit and model prediction error were evaluated by RMSE.

The PacIOOS turbidity plume forecast based on the Waikīkī ROMS predicts 3-dimensional circulation as well as salinity, temperature, and turbidity based on the PacIOOS NS02 measurements for the canal and adjacent coastal region. The model is spatially resolved within the canal and near-shore environment to 40 m with 14 depth layers (0.25, 1, 2, 5, 10, 20, 30, 50, 75, 100, 125, 150, 200, 250 m) at 1 h time intervals with a 3-day lead time. *V. vulnificus* density was predicted for the surface 0.25 m depth using the forecasted salinity and temperature, NWS 5-day average rainfall, and daily maximum air temperature.

2.6.5. Long-term forecasting

End-of-century projections of air temperature and precipitation were used to estimate overall change in *V. vulnificus* density due to climate change. The dynamical downscaling projections that were used (Zhang et al., 2012, 2016a, 2016b) are based on the IPCC AR5 CMIP5 global model for representative concentration pathways (RCP) 4.5 and 8.5 (IPCC, 2014). The forecasting assumes a linear response of *V. vulnificus* with increasing temperature and no significant changes to other aspects of environmental variation.

3. Results

3.1. Seasonal habitat variation

The 5-day average rainfall and 3-day average stream discharge preceding sampling events were not significantly different (n=9,t-tests, p>0.05)

between the nominal dry (Apr-Sep) and rainy season (Oct-Mar; Table 1). However, the highest 5-day average rainfall (23 mm d $^{-1}$ in Sep) and geometric mean (4.2 mm d $^{-1}$) for the dry season was higher than the highest value (21 mm d $^{-1}$ in Feb) and geometric mean (0.9 mm d $^{-1}$) for the rainy season for the events sampled. Daily maximum air temperature (n = 9) and water temperature for all sites and sampled depths (n = 206) were both significantly higher (t-tests, p < 0.05) in the dry versus rainy season (Table 1; Suppl. Fig. 2). Salinity (n = 206), chlorophyll (n = 197), and turbidity (n = 197) measured in situ for all sites and sampled depths were not significantly different (t-tests, p > 0.05) between the dry and rainy seasons. Dissolved oxygen (n = 205) measured in situ for all sites and sampled depths was significantly higher (t-test, p < 0.05) in the dry versus rainy season.

3.2. Spatial and temporal variation of Vibrio vulnificus

The overall average qPCR assay efficiency was 102 (range of 97–108) with an average R^2 of 0.97 (range of 0.94–0.99), slope of –3.3 (range of –3.4 to –3.2) and intercept of 41 (range 39–41). *V. vulnificus* concentration for all sites and sampled depths was significantly higher (t-test, p < 0.0001) in the nominal dry (n = 82) versus rainy (n = 89) season. The highest concentration (512 vvhA gene copies mL^{-1}) and geometric mean (30 vvhA gene copies mL^{-1}) for samples collected during the dry season was higher than the highest concentration (333 vvhA gene copies mL^{-1}) and geometric mean (6.4 vvhA gene copies mL^{-1}) for the rainy season. There were significant differences in V. vulnificus concentration between months, sites, and sample collection depths (ANOVA, p < 0.01). There were significant interactions between site and sample collection depth as well as site and month (ANOVA, p < 0.01). V. vulnificus concentration was significantly elevated in the surface water, within the canal (sites 3–8), and months during the dry season (Fig. 2).

3.3. Correlation with biogeochemical predictors

 $V.\ vulnificus$ concentration was most strongly correlated with dissolved inorganic nutrient concentrations and metrics of fluorescent DOM characteristics (Suppl. Fig. 1; r>0.6). Additional univariate correlations (r>0.4) were 5-day average rainfall, total prokaryote concentration, turbidity (Suppl. Fig. 2), and bulk measurements of dissolved and particulate organic carbon and nitrogen. $V.\ vulnificus$ concentration was strongly negatively correlated (r<-0.4) with pH and salinity. $V.\ vulnificus$ concentration was not significantly correlated (p>0.05) with 3-day average stream discharge and chlorophyll concentration measured in situ.

3.4. Predictive model selection

To construct predictive models, highly correlated biogeochemical variables were removed to mitigate overfitting, unstable coefficient estimates, and high prediction error. We prioritized parameters that are widely measured, lower cost and available on continuous monitoring platforms. Out of 36 biogeochemical measurements, 12 were chosen for model selection

Table 1Seasonal habitat variation assessed by the nominal dry and rainy seasons.

Measurement	Nominal Dry Season (Apr-Sep)				Nominal Rainy Season (Oct-Mar)				t-test	
	n	Geometric Mean	95% Confidence Interval		n	Geometric Mean	95% Confidence Interval		<i>p</i> -value	
5-Day Average Rainfall (mm d ⁻¹)	4	4.2	0.5	38	5	0.9	0.1	6.6	0.260	
3-Day Average Stream Discharge (m ³ s ⁻¹)	4	0.3	0.1	0.4	5	0.4	0.2	0.5	0.390	
Daily Max Air Temperature (°C)	4	32	30	34	5	29	27	31	0.032	*
Water Temperature (°C)	96	28	28	28	110	26	26	26	<<0.001	***
Salinity	96	30	29	31	110	30	29	31	0.720	
Chlorophyll (μg L ⁻¹)	90	1.3	0.9	1.9	107	1.7	1.2	2.3	0.380	
Turbidity (NTU)	90	2.5	2.0	3.1	107	1.9	1.6	2.3	0.067	
Dissolved Oxygen (mg L ⁻¹)	95	7.1	6.6	7.6	110	6.2	5.7	6.7	0.012	*

n = the number of observations; Significance codes are based on *p*-values: 0 '***' 0.001 '**' 0.01 '*' 0.05 '.'

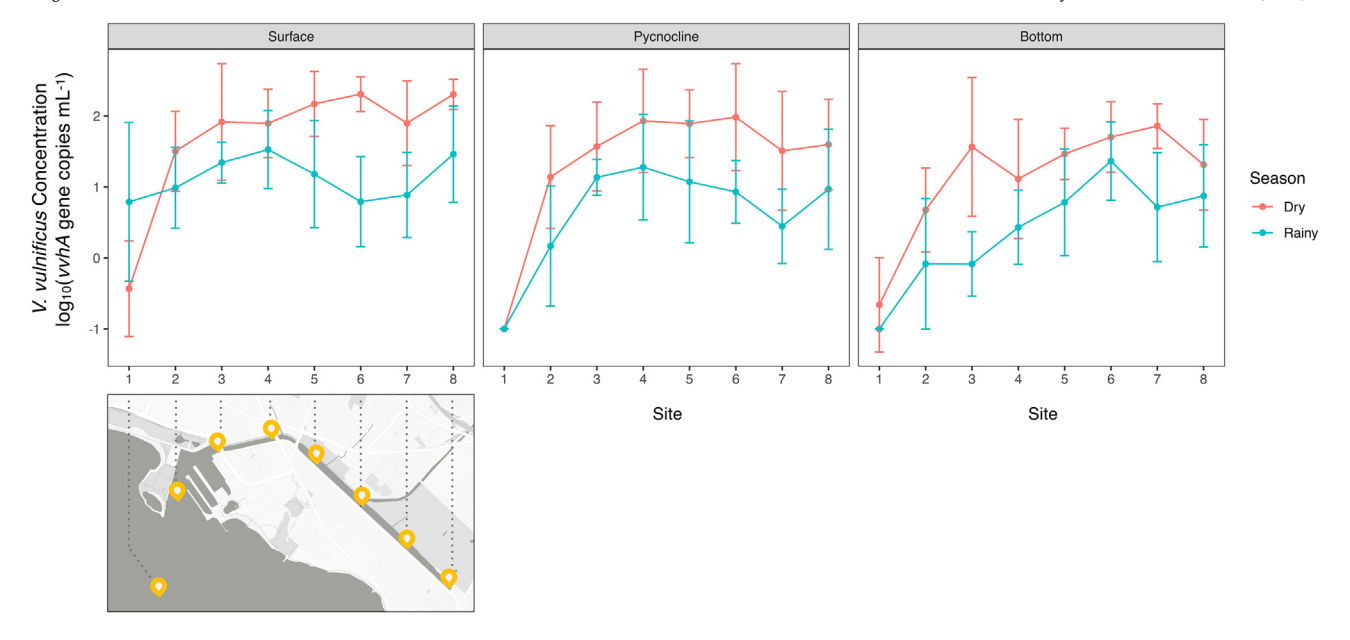


Fig. 2. Spatial and temporal variation of *V. vulnificus* density in the Ala Wai Canal in Honolulu, Hawai'i from October 2018–September 2019 divided by site (horizontal axis), season (color), and sample depth (panels). Error bars show the 95% confidence interval. *V. vulnificus* density varies significantly between seasons, sites, and depths (*p* < 0.001). *V. vulnificus* density significantly increases from offshore (site 1) to the back end of the canal (site 8) and in the surface waters (0.25 m from the surface) relative to the pycnocline or bottom waters (0.25 m from the bottom).

analysis, with 1-2 parameters each representing one of 9 clusters of covarying parameters (Suppl. Fig. 1). Although correlated, water temperature and air temperature capture different aspects of environmental variation (finescale horizontal and vertical spatial resolution versus broad seasonal weather patterns, respectively). Inclusion of both predictors did not cause issues of multicollinearity assessed by variance inflation factors in the models. Log₁₀(5-day average rainfall), daily maximum air temperature. water temperature, dissolved oxygen, squared(salinity), log₁₀(turbidity), log₁₀(chlorophyll), log₁₀(particulate organic carbon), log₁₀(nitrate plus nitrite), log₁₀(total phosphorus), log₁₀(visible humic-like DOM), and the DOM humification index (HIX) were used as terms to construct a linear model of V. vulnificus density in $log_{10}(vvhA gene copies mL^{-1})$ (Table 2). Model residuals were well-behaved (uniformly distributed relative to predicted values) and normally distributed, following model assumptions. For the full model with all terms, the residual standard error was 0.44 on 141 degrees of freedom with an R² value of 0.79 (Table 2).

Five models had a $\Delta AICc < 2$ from the best-specified model compared to models of all possible combinations of predictors. The importance value for each predictor, calculated using the MuMIn package, are reported in

Table 2. The best-specified model, based on the lowest AICc, included $\log_{10}(5\text{-day}$ average rainfall), daily maximum air temperature, water temperature, $\log_{10}(\text{nitrate}$ plus nitrite), $\log_{10}(\text{visible}$ humic-like DOM), and the DOM humification index (HIX). Variance inflation factors (VIF) were <5 for all model terms in the best-specified model. The residual standard error was 0.44 on 157 degrees of freedom with an R^2 value of 0.80 (Model 6 in Table 3).

3.5. Operational model comparison and cross validation

Table 2Linear regression analysis of *V. vulnificus* density in $\log_{10}(vvhA$ gene copies mL⁻¹) and AIC-weighted importance of predictors.

Model Term	Coefficient Estimate	95% Confidence Interval		Standard Error	t-value	p-value	Significance	Importance
(Intercept)	4.3E+0	2.6E+0	6.0E + 0	8.7E-1	5.0	2.10E - 06		
log ₁₀ Visible Humic-like DOM	2.0E + 0	1.4E + 0	2.6E + 0	2.9E - 1	7.0	1.10E - 10	***	1.00
Daily Max Air Temperature	1.9E - 1	1.4E - 1	2.5E - 1	2.8E - 2	6.8	2.20E - 10	***	1.00
DOM Humification Index (HIX)	-3.1E-1	-4.0E-1	-2.2E-1	4.5E - 2	-6.8	2.40E - 10	***	1.00
log ₁₀ 5-Day Average Rainfall	3.5E - 1	2.4E - 1	4.6E - 1	5.7E - 2	6.1	1.00E - 08	***	1.00
log ₁₀ Nitrite + Nitrate	6.1E - 1	4.0E - 1	8.2E - 1	1.1E - 1	5.8	3.90E - 08	***	1.00
Water Temperature	-2.3E-1	-3.2E-1	-1.5E-1	4.3E - 2	-5.4	2.40E - 07	***	1.00
Dissolved Oxygen	-1.2E-2	-4.1E-2	1.7E - 2	1.5E - 2	-0.8	4.30E - 01		0.36
Log ₁₀ Turbidity	1.0E - 1	-1.4E-1	3.5E - 1	1.2E - 1	0.8	4.10E - 01		0.35
Squared Salinity	9.2E-5	-4.0E-4	5.9E - 4	2.5E - 4	0.4	7.10E - 01		0.28
log ₁₀ Particulate Organic Carbon	-4.2E-2	-3.5E-1	2.6E - 1	1.5E - 1	-0.3	7.90E - 01		0.27
log ₁₀ Total Phosphorus	-4.0E-2	-4.6E-1	3.8E - 1	2.1E - 1	-0.2	8.50E - 01		0.25
log ₁₀ Chlorophyll	-6.0E - 3	-1.4E-1	1.3E - 1	6.8E - 2	-0.1	9.30E - 01		0.25

Significance codes are based on p-values: 0 '***' 0.001 '**' 0.01 '*' 0.05 '.'

Table 3 Comparative linear regression analysis of V. vulnificus density in $log_{10}(vvhA$ gene copies mL^{-1}) between six operational models.

Model 1 "Weather"	$R^2 = 0.25$	$\Delta AICc = 204$	RMSE = 0.82	LOOCV- RMSE = 0.84	PE = 6.9	n = 164	
Model Term	Estimate 95% Confidence Interval		Standard Error	t-value	p-value	Significanc	
(Intercept)	-3.2E + 0	-4.8E + 0	-1.5E + 0	8.3E - 1	-3.8	2.00E-04	
log ₁₀ 5-Day Average Rainfall	4.0E - 1	2.4E - 1	5.6E - 1	8.3E - 2	4.8	3.30E-06	***
Daily Max Air Temperature	1.4E - 1	8.3E - 2	1.9E - 1	2.7E - 2	5.0	1.40E - 06	***
				LOOCV -			
Model 2 "Chemistry"	$R^2 = 0.45$	$\Delta AICc = 154$	RMSE = 0.71	RMSE = 0.72	PE = 5.3	n = 164	
Model Term	Estimate 95% Confidence Interval		Standard Error	t-value	p-value	Significano	
(Intercept)	-2.3E + 0	-3.8E + 0	-8.4E - 1	7.6E - 1	-3.1	2.50E - 03	
Squared Salinity	-2.0E - 3	-2.4E - 3	-1.6E - 3	2.0E - 4	-10.0	2.00E - 16	***
Water Temperature	1.9E - 1	1.3E - 1	2.5E - 1	2.8E - 2	6.7	2.90E - 10	***
				LOOCV -			
Model 3 "Weather + Chemistry	$\underline{Y''} \qquad \underline{R^2 = 0.51}$	$\Delta AICc = 138$	RMSE = 0.67	RMSE = 0.69	PE = 4.9	n = 164	
Model Term	Estimate	95% Confidence	ce Interval	Standard Error	t-value	p-value	Significano
(Intercept)	-2.5E + 0		-1.0E + 0	7.5E - 1	-3.4	9.50E - 04	
log ₁₀ 5-Day Average Rainfall	2.4E - 1	1.0E - 1	3.8E - 1	7.2E - 2	3.4	9.60E - 04	***
Daily Max Air Temperature	1.3E - 1	5.8E - 2	2.0E - 1	3.7E - 2	3.6	4.90E - 04	***
Squared Salinity	-1.8E - 3		-1.4E - 3	1.9E - 4	-9.1	2.90E - 16	***
Water Temperature	4.1E – 2	-4.9E - 2	1.3E - 1	4.6E - 2	0.9	3.65E - 01	
				LOOCV -			
Model 4 "Model 3 + Nutrients	$R^2 = 0.55$	$\Delta AICc = 126$	$\frac{\text{RMSE} = 0.64}{\text{MSE}}$	RMSE = 0.66	$\underline{PE = 4.6}$	n = 164	
Model Term	Estimate	95% Confidence	e Interval	Standard Error	t-value	p-value	Significan
(Intercept)	-1.9E + 0	-3.3E + 0	-4.1E - 1	7.4E - 1	-2.5	1.24E-02	
log ₁₀ 5-Day Average Rainfall	2.9E - 1	1.5E - 1	4.3E - 1	7.0E - 2	4.2	5.40E - 05	***
Daily Max Air Temperature	1.7E - 1	9.8E - 2	2.4E - 1	3.7E - 2	4.6	7.20E - 06	***
Squared Salinity	- 9.7E - 4	-1.5E - 3	-4.2E-4	2.8E - 4	-3.5	6.60E - 04	***
Water Temperature	-6.4E - 2	-1.7E - 1	3.8E - 2	5.2E - 2	-1.2	2.20E - 01	
log ₁₀ Nitrite + Nitrate	5.4E - 1	2.6E - 1	8.2E - 1	1.4E - 1	3.8	2.10E – 04	***
	m ² 0.50			LOOCV-			
Model 5 "Model 3 + DOM" $R^2 = 0.68$		$\Delta AICc = 68 \qquad RMSE = 0.53$		RMSE = 0.55	PE = 3.6	n = 164	
Model Term	Estimate	95% Confidence	Interval	Standard Error	t-value	p-value	Significan
(Intercept)	6.6E - 1	-7.1E - 1	2.0E + 0	6.9E - 1	1.0	3.41E-01	***
log ₁₀ 5-Day Average Rainfall	3.7E - 1	2.6E - 1	4.9E - 1	6.0E - 2	6.3	3.20E – 09	***
Daily Max Air Temperature	2.0E - 1	1.4E - 1	2.6E - 1	3.1E - 2	6.7	4.60E – 10	***
Squared Salinity	-3.2E - 4	-7.6E - 4	1.1E - 4	2.2E - 4	-1.5	1.39E - 01	***
Water Temperature	-1.5E - 1	-2.3E - 1	-6.5E - 2	4.2E - 2	-3.5	5.40E - 04	***
log ₁₀ Visible Humic-like DOM	1.4E + 0	1.1E + 0	1.7E + 0	1.5E - 1	9.3	2.00E – 16	***
Model 6 "Deet ener; God"	$R^2 = 0.80$	AAICa — O	DMCE - 0.42	LOOCV -	DE - 2.0	164	
Model 6 "Best-specified"		$\Delta AICc = 0$	$\frac{\text{RMSE} = 0.43}{}$	RMSE = 0.45	$\frac{PE = 2.8}{}$	<u>n = 164</u>	
Model Term	Estimate	95% Confidenc		Standard Error	t-value	p-value	Significan
(Intercept)	3.9E + 0	2.6E + 0	5.2E + 0	6.6E - 1	6.0	1.70E – 08	
log ₁₀ 5-Day Average Rainfall	3.7E - 1	2.8E - 1	4.6E - 1	4.5E - 2	8.2	9.50E-14	***
Daily Max Air Temperature	1.9E - 1	1.4E - 1	2.4E - 1	2.4E - 2	7.7	1.80E - 12	***
Water Temperature	-2.2E - 1	-2.8E - 1	-1.6E - 1	3.1E - 2	-7.3	1.80E-11	***
log ₁₀ Nitrite + Nitrate	5.6E1	4.0E - 1	7.2E - 1	8.1E - 2	6.9	1.10E-10	***
DOM Humification Index (HIX)		-3.6E - 1	-2.2E - 1	3.6E - 2	-8.0	2.80E-13	***
log ₁₀ Visible Humic-like DOM	1.9E + 0	1.6E + 0	2.2E + 0	1.3E - 1	14.5	2.00E - 16	***

AICc = Akaike Information Criterion value corrected for small sample sizes. RMSE = average error between the predicted and observed value. LOOCV = leave-one-outcross-validation technique. PE = prediction error; the log-corrected RMSE from LOOCV. The data set, including the number of observations (n), was kept consistent to allow for model comparison. Significance codes are based on p-values: 0 '***' 0.001 '**' 0.01 '**' 0.05 '.'

= 0.84, PE = 6.9). Model 2 included water chemistry: squared(salinity) and water temperature. Model 2 explained more variation in *V. vulnificus* concentration with lower prediction error (R² = 0.45, Δ AICc = 154, RMSE = 0.71, LOOCV-RMSE = 0.72, PE = 5.3) than Model 1. Model 3 combined climate and water chemistry variables: $\log_{10}(5\text{-day})$ average rainfall), daily maximum air temperature, squared(salinity), and water temperature. Salinity and water temperature are measured in the PacIOOS NS02 time series and modeled in the Waikiki ROMS turbidity plume forecast, so Model 3 was applied to those nowcasting and forecasting frameworks. Model 3 explained more variation in *V. vulnificus* concentration with lower prediction error (R² = 0.51, Δ AICc = 138, RMSE = 0.67, LOOCV-RMSE = 0.69, PE = 4.9) than Model 2. Model 4 builds from Model 3 to

include $\log_{10}(\text{nitrate plus nitrite})$ to assess the impact of adding a dissolved nutrient predictor. Model 4 explained more variation in *V. vulnificus* concentration with lower prediction error (R² = 0.55, Δ AICc = 126, RMSE = 0.64, LOOCV-RMSE = 0.66, PE = 4.6) than Model 3. To assess the impact of adding a dissolved organic matter predictor, Model 5 builds from Model 3 to include $\log_{10}(\text{visible humic-like DOM})$ which is an additional measurement collected continuously at the Pacioos NS02. Model 5 explained more variation in *V. vulnificus* concentration with lower prediction error (R² = 0.68, Δ AICc = 68, RMSE = 0.53, LOOCV-RMSE = 0.55, PE = 3.6) than Models 3 and 4. Model 6 is the best-specified model from model selection analysis (R² = 0.80, Δ AICc = 0, RMSE = 0.43, LOOCV-RMSE = 0.45, PE = 2.8). All of the models, including Model 6, slightly

overestimate *V. vulnificus* concentration when observations of *V. vulnificus* concentration are near or below the detection limit (Suppl. Fig. 3).

3.6. Model forecasting applications

3.6.1. Short-term forecasting

The PacIOOS time series data from NS02 were validated against measured observations in this survey from site 2 at 0.75 to 2 m depth (Suppl. Fig. 4). Overall, the NS02 data were roughly equivalent to the survey data with high R² values and a linear fit with intercepts near zero and slopes near one. Salinity was an exception with an R² of 0.41, possibly attributable to fine-scale variation in sampling location in a stratified estuarine habitat. Using the NS02 data, V. vulnificus concentration was hindcast for the sampling period (Suppl. Fig. 5) and validated against measured observations (Suppl. Fig. 6). Two model frameworks were compared to assess the improvement of adding DOM measurements (Model 3 vs. Model 5, see Section 3.5). There were 5 sampling events which overlapped with the NS02 fDOM sensor in operation. For those 5 measurements of V. vulnificus concentration at site 2 and surface depths, Model 3 and Model 5 (Model 3 + DOM) parameters were applied to make predictions of V. vulnificus concentration (Suppl. Fig. 6). Compared to observations, predictions based on Model 5 ($R^2 = 0.83$, RMSE = 0.31, PE = 2.0) were improved over Model 3 ($R^2 = 0.03$, RMSE = 0.44, PE = 2.8).

In addition to the time series at NSO2, a 3-day spatially-resolved forecast of *V. vulnificus* density was constructed using the PacIOOS turbidity plume forecast and Waikīkī ROMS model framework which includes 4 m resolution projections of salinity and temperature in addition to water velocity at 1 h intervals. Model 3 (see Section 3.5) was used to predict *V. vulnificus* density based on the plume forecast output. For an example rain event in February 2019, this model demonstrated *V. vulnificus* plume dynamics exiting the Ala Wai Canal (Fig. 3).

3.6.2. Long-term forecasting

Long-term climate-based predictions of V. vulnificus were based on Model 1 using projections of monthly average rainfall and air temperature. Inclusion of local water chemistry predictions would be ideal to parameterize the model but are not currently available. Model 1 was first validated against survey measurements of V. vulnificus density (Fig. 4). The climate model does not accurately predict the spatial variation in V. vulnificus density ($R^2 = 0.25$, RMSE = 0.82, PE = 6.9), but does well to predict the overall average V. vulnificus density within the canal ($R^2 = 0.90$, RMSE = 0.04, PE = 1.1). Model coefficients were used to predict the long-term effects of changing rainfall and air temperature on overall average V. vulnificus density for the canal. Three climate projections were considered based on dynamical downscaling (250 m resolution) of recorded data (1990-2009) and the AR5 RCP 4.5 and RCP 8.5 modeled scenarios (2080-2099). RCP 4.5 is a 580–720 ppm CO2-eq by 2100 and 1.7–3.2 °C increase relative to 1850–1900 and RCP 8.5 is a > 1000 ppm CO2-eq by 2100 and 3.2–5.4 °C increase relative to 1850–1900. There was no significant difference (p =0.86) in annual average rainfall between the three projections (1990–2009, RCP 4.5, and RCP 8.5) (Suppl. Fig. 7). There was a significant difference (p < 0.0001) in annual average air temperature between the three projections. Mean comparisons using Tukey-Kramer HSD show that RCP 8.5 (mean = 28 °C) is significantly higher (p < 0.0001) than RCP 4.5 (mean = 26 °C) and RCP 4.5 is significantly higher (p < 0.0001) than 1990–2009 (mean = 24 °C). There is also a significant difference (p < 0.0001) in predicted annual average V. vulnificus density between the three projections (Suppl. Fig. 7; Fig. 5). Mean comparisons using Tukey-Kramer HSD show that RCP 8.5 (geometric mean = 120 vvhA gene copies mL^{-1}) is significantly higher (p < 0.0001) than RCP 4.5 (geometric mean = 69 vvhA gene copies mL⁻¹) and RCP 4.5 is significantly higher (p < 0.0001) than 1990-2009 (geometric mean = 36 vvhA gene copies mL⁻¹). The mean RCP 4.5 and 8.5 values in V. vulnificus density correspond

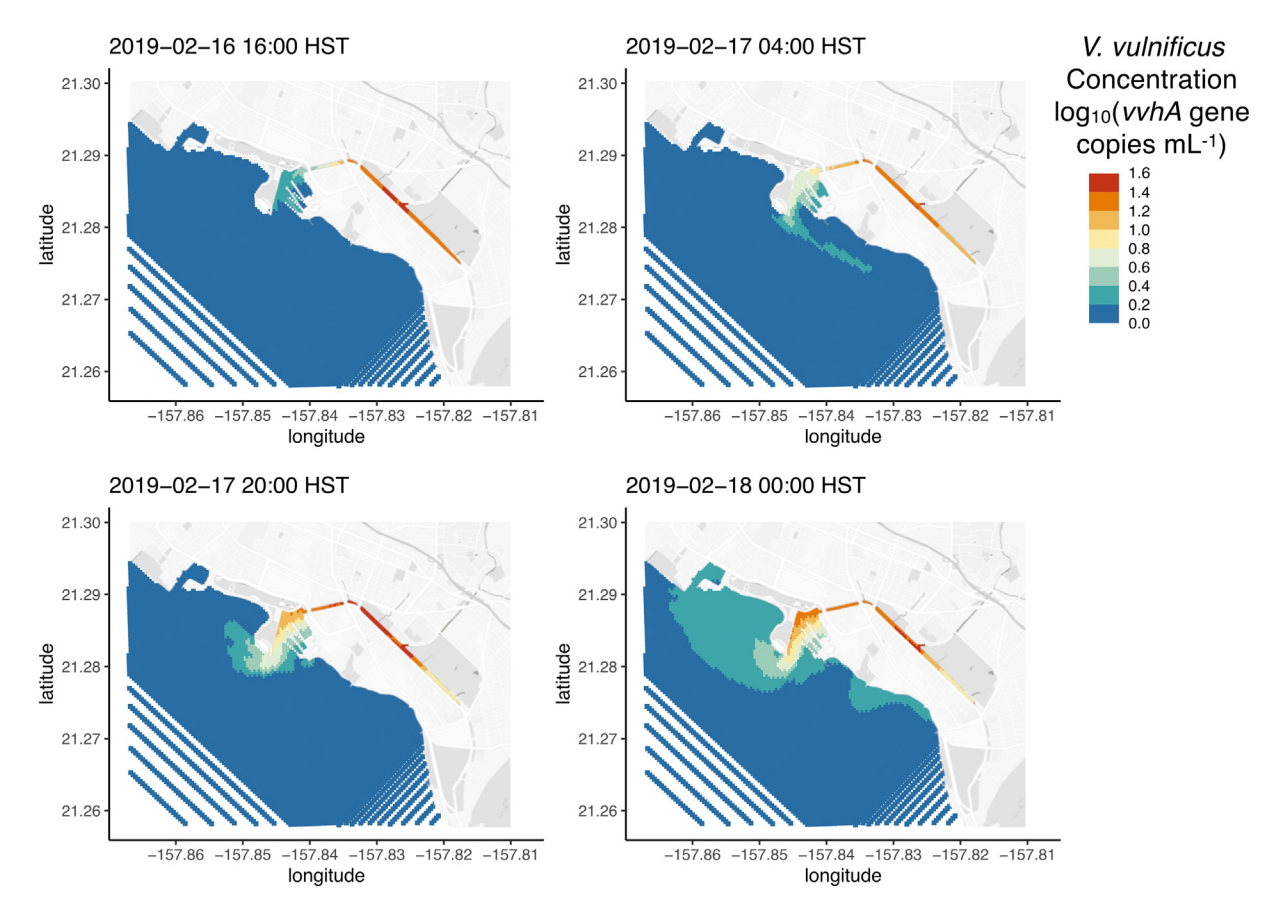


Fig. 3. Applied model predictions (Table 2, Model 3) using the PaciOOS turbidity plume forecast showing surface plume dynamics of *V. vulnificus* density into recreational areas during a rain event (16–18 of February 2019).

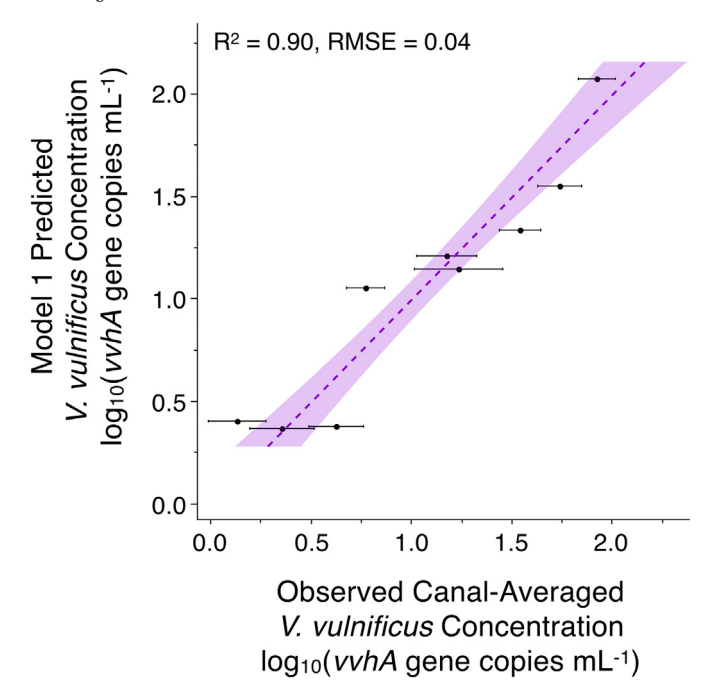


Fig. 4. Model-predicted *V. vulnificus* density based on rainfall and air temperature compared to measured *V. vulnificus* density within the canal (sites 2–8). Measured *V. vulnificus* density is shown as the geometric mean with standard error around the mean value. The linear fit ($y = 1 \times -3.55E-15$) is practically 1:1 and the 95% confidence interval is shaded. The climate-based model does not predict the spatial variation in *V. vulnificus* density ($R^2 = 0.42$, RMSE = 0.65, *PE = 4.47), but expertly predicts the overall monthly average of *V. vulnificus* density within the canal ($R^2 = 0.90$, RMSE = 0.04, PE = 1.1).

to a 1.9 and 3.3-fold increase, respectively, relative to the mean for 1990–2009 (Fig. 5).

4. Discussion

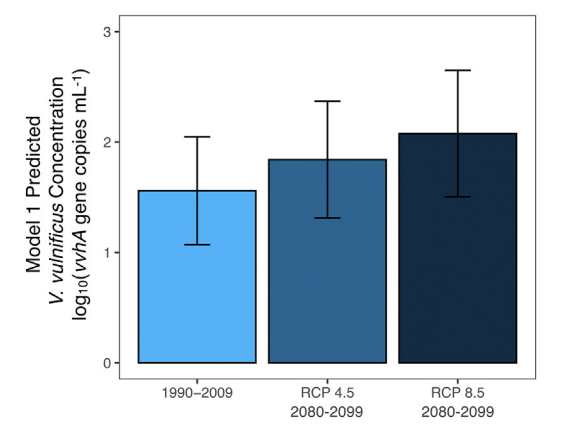
4.1. General patterns in Vibrio vulnificus abundance and seasonality

This study evaluates statistical models of *V. vulnificus* concentrations in the Ala Wai Canal, a tropical estuarine environment in a densely populated area of Honolulu, Hawai'i. The results demonstrate that accounting for

spatiotemporal dynamics of dissolved nutrient and organic matter resources resulted in high predictive capability for a statistical model in this tropical estuarine system. Despite the high degree of both temporal and spatial variation, weather and biogeochemistry explained 80% of the variation in *V. vulnificus* concentration using the best-specified model (Model 6 in Table 3) which includes $\log_{10}(5\text{-day}$ average rainfall), daily maximum air temperature, water temperature, $\log_{10}(\text{nitrate plus nitrite})$, $\log_{10}(\text{visible humic-like DOM})$, and the DOM humification index (HIX). At low *V. vulnificus* concentrations, this model tends to slightly overestimate concentrations (see Model 6 in Suppl. Fig. 3). For environmental systems without sustained populations of *V. vulnificus* year-round, such as the Chesapeake Bay, model implementation may need to be paired with a binomial model of presence and absence to verify accurate predictions near the detection limit.

The significantly higher average abundance of V. vulnificus in the months of the nominal dry season during this study contrasts with findings from a study of the canal a decade prior (Nigro et al., 2022). In the 2008–2009 study, V. vulnificus abundance was significantly higher on average during the rainy season, but also more variable. The authors concluded that rainfall, by modulating salinity in the canal, was the principal control on V. vulnificus abundance. Although there is a climatological rainy season in Hawai'i (Giambelluca et al., 2013), rainfall events are highly variable within and between years. Unlike the prior study, there was no significant difference in average rainfall or salinity for samplings during the nominal rainy vs. dry months in this study. The highest rainfall event captured (23 mm d^{-1} of a 5-day average preceding water sampling) was at the end of the nominal dry season (late September) and the geometric mean was ~5-fold higher in the nominal dry season. This is likely attributable to deviations from long-term seasonal patterns in rainfall, as well as limited temporal resolution of sampling. In the absence of a strong seasonal signal in rainfall, the highest V. vulnificus abundances were observed in the warmer, summer months when organic carbon concentrations were also elevated.

These seemingly contrasting results between studies of the same habitat highlight the importance of stochastic rain events in controlling the abundance of *V. vulnificus* in this system and underscores the importance of developing accurate predictive models. Baseline abundances of *V. vulnificus* are higher in the warmer, more stable summer months, but episodic rain events – which can happen at anytime, albeit more common in the rainy season – can result in pulses of high *V. vulnificus* density. Rain events, which transport nutrients and dissolved organics as well as low salinity water into the canal through the streams and runoff, are positively correlated with *V. vulnificus* density (see the February 2019 rain event in Fig. 3). These findings are consistent with Nigro et al. (2022). Both studies



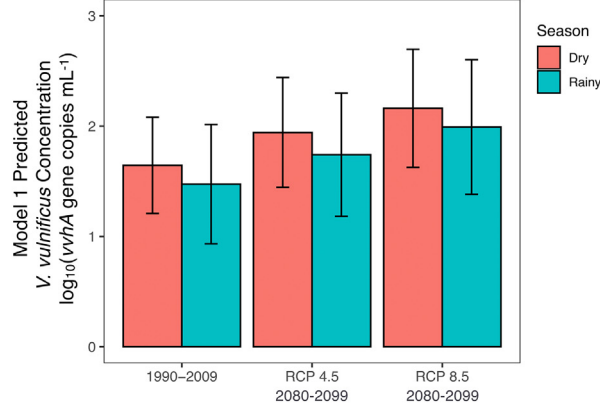


Fig. 5. Predicted V. vulnificus density from monthly average climate projections of rainfall and air temperature based on dynamical downscaling (250 m resolution) of recorded data (1990–2009) and the AR5 RCP 4.5 and RCP 8.5 modeled scenarios* (2080–2099). The right panel separates the data by season (colors). Error bars show the 95% confidence interval. There is a significant increase (p < 0.0001) in predicted average V. vulnificus density between the 1990–2009 data and the RCP 4.5 projection and also between the RCP 4.5 projection and the RCP 8.5 projection. There is a significant effect of season (p < 0.001) for the 1990–2009 data and projected scenarios, but no significant interaction (p > 0.05) between scenario and season. *The Intergovernmental Panel on Climate Change (IPCC) 5th Assessment Report 2014. Representative Concentration Pathways. RCP 4.5: 580–720 ppm CO_2 -eq by 2100 and 1.7–3.2 °C increase relative to 1850–1900. RCP 8.5: >1000 ppm CO_2 -eq by 2100 and 3.2–5.4 °C increase relative to 1850–1900.

show elevated concentrations of *V. vulnificus* in the harbor region after a large rain event. Since the harbor and outflow regions are sites of high and concentrated recreational activity, summer rain storms may be particularly concerning for human exposure to *V. vulnificus*. Fiedler et al. (2014) also reported a significant increase in *V. vulnificus* density near the PaciOOS NS02 following the March 2011 Japan tsunami. The importance of the DOM humification index (HIX) in the modeling exercises may also suggest a response of *V. vulnificus* to groundwater flow. Nelson et al. (2015) show that elevated HIX values can be an indicator of submarine groundwater discharge.

The pattern and order-of-magnitude seasonal variation in *V. vulnificus* density recorded in this study is comparable to previous studies in other areas (Jacobs et al., 2014; Pfeffer et al., 2003; Tamplin et al., 1982). However, in the tropical waters of the Ala Wai Canal, water temperature (ranging between 22 and 31 °C during this study) permits population growth year-round. Additional aspects of environmental variation significantly affect the temporal and spatial patterns of abundance. Considered together, salinity and temperature explained only 40% of the variation in *V. vulnificus* density.

4.2. Improving predictions with dissolved nutrients and organics

The quality of nutrient resources available to V. vulnificus cells may be an important and overlooked determinant in predicting the population dynamics of V. vulnificus. Our results indicate that the addition of fluorescent dissolved organic matter (fDOM) measurements to resolve humic components (often targeting a range of wavelengths referred to as "cDOM" or visible humic-like components; Nelson and Siegel, 2013) could resolve 17% more variation in V. vulnificus density than salinity, water temperature, and weather alone (Model 5 vs. 3 in Table 2). In application, the addition of a real-time deployed fDOM sensor at NS02 reduced prediction error by 29% (Suppl. Fig. 6). Although dissolved inorganic nutrients are also important in the models (Model 4 vs. 3 increases V. vulnificus variation explained by 4%) and are strongly correlated with V. vulnificus concentrations, nutrient analysis currently requires water sample collection and laboratory analysis. Fluorescent DOM can be measured with a deployed real-time sensor and fDOM parameters were almost equally correlated with V. vulnificus (Suppl. Fig. 1). However, advances are being made in real-time sensors for inorganic nutrients such as nitrate (Sea-Bird Scientific, SUNA V2 Nitrate Sensor based on Johnson and Coletti, 2002) and orthophosphate (Sea-Bird Scientific, HydroCycle-Phosphate Analyzer). These real-time sensors of DOM and nutrients may become valuable tools for future coastal pathogen monitoring programs.

There are only a few studies on natural populations of V. vulnificus in tropical estuaries. In the case of a tropical environment where warmer water temperature is always permitting growth, other factors, such as macronutrient resource abundance and quality, may be more important controls on the population density of V. vulnificus. Vibrios are copiotrophic bacterioplankton with broad capacity to degrade organic compounds and extract macronutrients from DOM (Baker-Austin et al., 2018). As such, the character and quantity of DOM is a reasonable parameter modulating growth dynamics of this pathogen and other naturally-occurring estuarine organisms. Considering nutrient and DOM resources in predictive modeling seems to be a promising route forward. Measurements of fluorescent DOM, which can be recorded easily with deployed sensors (Belzile et al., 2006; Carstea et al., 2020; Ruhala and Zarnetske, 2017), may be the key to generating robust predictive models of V. vulnificus population dynamics. There are even promising efforts at forecast modeling DOM in estuarine environments (Bowers and Brett, 2008) which could be integrated into coastal pathogen modeling.

4.3. Conclusions and climate change implications

This study parameterizes *V. vulnificus* absolute abundance with comprehensive physical, optical, and chemical water properties in high spatial and temporal resolution to develop a real-time spatially-explicit model of

V. vulnificus pathogen risk. It is critical that we improve our predictive capabilities of the V. vulnificus human pathogen in the face of increased water temperature, storm surge, sea level, hurricanes, and flooding due to climate change which may be favorable to V. vulnificus. The habitat range of V. vulnificus may expand landward in this system due to sea level rise and coastal flooding (https://www.pacioos.hawaii.edu/shoreline/slr-hawaii/) given its preference for mixed salinity water. In addition, V. vulnificus population growth rates will likely increase due to increasing water temperature. There is evidence for significantly increased length of seasonal occurrence and spatial habitat from research in the Chesapeake Bay (Muhling et al., 2017). Based on local dynamical downscaling of the CMIP5 global model projections for rainfall and air temperature (Zhang et al., 2012, 2016a, 2016b), our models suggest a 2- to 3-fold increase in average V. vulnificus density in the Ala Wai Canal by 2100 if atmospheric CO₂ concentrations reach between RCP 4.5 and 8.5. However, these model projections are limited to climate variables and assume a linear response of V. vulnificus. A nuanced modeling approach including predictions of water chemistry, which are not yet resolved at a fine-scale local level in this system, and the variability of stochastic weather events as well as societal response will be necessary to forecast the long-term dynamics of V. vulnificus density. If climate change proves more favorable for V. vulnificus and expands areas of coastal flooding, we will likely see increased exposure of the general public to V. vulnificus and increased infections. Therefore, improving predictive models of microbial pathogen populations is essential for public safety and incorporating real-time measurements of dissolved nutrient and organic matter resources may be a crucial step forward.

CRediT authorship contribution statement

Jessica A. Bullington, Data curation, Formal analysis, Investigation, Methodology, Project administration, Software, Supervision, Validation, Visualization, Writing - original draft (in totality), Writing - review & editing

Abigail R. Golder, Data curation, Investigation, Methodology, Writing - original draft (methodology), Writing - review & editing

Grieg F. Steward, Conceptualization, Funding acquisition, Methodology, Resources, Writing - review & editing

Margaret A. McManus, Conceptualization, Funding acquisition, Methodology, Resources, Writing - review & editing

Anna B. Neuheimer, Conceptualization, Formal analysis, Funding acquisition, Methodology, Software, Writing - review & editing

Brian T. Glazer, Funding acquisition, Investigation, Resources, Supervision

Olivia D. Nigro, Methodology, Resources, Writing - review & editing Craig E. Nelson, Conceptualization, Funding acquisition, Methodology, Project administration, Resources, Supervision, Writing - review & editing

Declaration of competing interest

The authors declare that they have no known competing financial interests or personal relationships that could have appeared to influence the work reported in this paper.

Acknowledgments

We thank the many technicians, interns, and volunteers who assisted with collection of samples from the canal: Stanley Lio, Solomon Chen, Shaun Wriston, Han Quach, Eleanor Yuan, Wesley Sparagon, Rayna McClintock, Brenna Carroll, Sarah Michal Hamid, Brianna Ornelas, Seraphina King, Justin Higa, Cory Yap, Sarah Cory, Kira Webster, Alex Quiroz, Ashley Hiʻilani Sanchez, Kyle Conner, Aka Beebe, Sean Mahaffey, Petra Byl, Cherise Spotkaeff, Isabelle Yazel Eiser, Nick Yoshioka, Kelsey Nichols, Zoe Glenn, Olivia Hughes, Maria Steadmon, Ashley Ostendorf, Sherine Boomla, and Sienna Santiago. We thank Danielle Hull who processed the nutrient samples at the SOEST Lab for Analytical Biogeochemistry, Kirsten

Nakayama and Nicole Yoneishi who assisted with DNA extractions at the UH Microbial Genomics and Analytical Lab, and Abby Frazier who assisted with accessing the downscaled climate change projections. We thank PaclOOS and Gordon Walker for providing and maintaining real-time data from NSO2 and Brian Powell for creating and maintaining the turbidity plume model forecast.

Funding

This work was supported by the University of Hawai'i at Mānoa SMART Ala Wai Program (Strategic Monitoring and Resilience Training in the Ala Wai Watershed), the National Science Foundation (OCE1737357; OCE1949033), the UH Microbial Genomics and Analytical Lab sponsored by NIH COBRE P20 (GM125508), an Aarhus University Research Foundation Starting Grant to A.B.N., and a grant/cooperative agreement from the National Oceanic and Atmospheric Administration, Project R/HE35, which is sponsored by the University of Hawai'i Sea Grant College Program, SOEST, under Institutional Grant No. NA18OAR4170076 from NOAA Office of Sea Grant, Department of Commerce. The views expressed herein are those of the authors and do not necessarily reflect the views of NOAA or any of its subagencies. This is UH Sea Grant publication number UNIHI-SEAGRANT-JC-19-21 and SOEST publication number 11478.

Supplementary Information

Supplementary figures and information for this article can be found online at https://doi.org/10.1016/j.scitotenv.2022.154075.

References

- Akaike, H., 1973. Information theory and an extension of the maximum likelihood principle. In: Parzen, E., Tanabe, K., Kitagawa, G. (Eds.), Selected Papers of Hirotugu Akaike. Springer Series in Statistics (Perspectives in Statistics), pp. 199–213 https://doi.org/10. 1007/978-1-4612-1694-0_15.
- Antone, R., 2006. The family wants answers to a man's rapid, "horrible death". Honolulu Star-Bulletin. http://archives.starbulletin.com/2006/04/08/news/story03.html. (Accessed 8 March 2022).
- Armstrong, F.A.J., Stearns, C.R., Strickland, J.D.H., 1967. The measurement of upwelling and subsequent biological process by means of the technicon Autoanalyzer® and associated equipment. Deep-Sea Res. Oceanogr. Abstr. 14 (3), 381–389. https://doi.org/10.1016/0011-7471(67)90082-4.
- Baker-Austin, C., Trinanes, J.A., Taylor, N.G.H., Hartnell, R., Siitonen, A., Martinez-Urtaza, J., 2013. Emerging Vibrio risk at high latitudes in response to ocean warming. Nat. Clim. Chang. 3 (1), 73–77. https://doi.org/10.1038/nclimate1628.
- Baker-Austin, C., Oliver, J.D., Alam, M., Ali, A., Waldor, M.K., Qadri, F., Martinez-Urtaza, J., 2018. Vibrio spp. infections. Nat. Rev. Dis. Primers. 4 (1), 1–19. https://doi.org/10. 1038/s41572-018-0005-8.
- Banakar, V., Constantin de Magny, G., Jacobs, J., Murtugudde, R., Huq, A., Wood, R.J., Colwell, R.R., 2011. Temporal and Spatial Variability in the Distribution of Vibrio vulnificus in the Chesapeake Bay: A Hindcast Study. EcoHealth 8, 456–467. https://doi. org/10.1007/s10393-011-0736-4.
- Bartoń, K., 2019. MuMIn: multi-model inference. R package version 1.43.6. https://CRAN.R-project.org/package=MuMIn.
- Belzile, C., Roesler, C.S., Christensen, J.P., Shakhova, N., Semiletov, I., 2006. Fluorescence measured using the WETStar DOM fluorometer as a proxy for dissolved matter absorption. Estuar. Coast. Shelf Sci. 67 (3), 441–449. https://doi.org/10.1016/j.ecss.2005.11. 032
- Bowers, D.G., Brett, H.L., 2008. The relationship between CDOM and salinity in estuaries: an analytical and graphical solution. J. Mar. Syst. 73 (1–2), 1–7. https://doi.org/10.1016/j. imarsvs.2007.07.001.
- Bullington, J.A., 2022. jessicabullington/AlaWai-vvhA-2018-2019: Release for publication (v1.0.0). Zenodo https://doi.org/10.5281/zenodo.6345513.
- Bustin, S.A., Benes, V., Garson, J.A., Hellemans, J., Huggett, J., Kubista, M., Mueller, R., Nolan, T., Pfaffl, M.W., Shipley, G.L., Vandesompele, J., Wittwer, C.T., 2009. The MIQE guidelines: minimum information for publication of quantitative real-time PCR experiments. Clin. Chem. 55 (4), 611–622. https://doi.org/10.1373/clinchem.2008.112797.
- Cai, W.J., 2011. Estuarine and coastal ocean carbon paradox: CO2 sinks or sites of terrestrial carbon incineration? Annu. Rev. Mar. Sci. 3, 123–145. https://doi.org/10.1146/annurevmarine-120709-142723.
- Campbell, M.S., Wright, A.C., 2003. Real-time PCR analysis of Vibrio vulnificus from oysters. Appl. Environ. Microbiol. 69 (12), 7137–7144. https://doi.org/10.1128/AEM.69.12. 7137-7144.2003.
- Carstea, E.M., Popa, C.L., Baker, A., Bridgeman, J., 2020. In situ fluorescence measurements of dissolved organic matter: a review. Sci. Total Environ. 699, 134361. https://doi.org/10. 1016/j.scitotenv.2019.134361.

- Centers for Disease Control and Prevention, 2014. National Center for Emerging and Infectious Diseases. National Enteric Disease Surveillance: Cholera and Other Vibrio Illness Surveillance (COVIS) Annual Summary. https://www.cdc.gov/vibrio/surveillance.html.
- Chen, C.Y., Wu, K.M., Chang, Y.C., Chang, C.H., Tsai, H.C., Liao, T.L., Liu, Y.M., Chen, H.J., Shen, A.B.T., Li, J.C., Su, T.L., Shao, C.P., Lee, C.T., Tsai, S.F., 2003. Comparative genome analysis of Vibrio vulnificus, a marine pathogen. Genome Res. 13 (12), 2577–2587. https://doi.org/10.1101/gr.1295503.
- Coble, P.G., 1996. Characterization of marine and terrestrial DOM in seawater using excitation-emission matrix spectroscopy. Mar. Chem. 51 (4), 325–346. https://doi.org/ 10.1016/0304-4203(95)00062-3.
- Connolly, J.P., Blumberg, A.F., Quadrini, J.D., 1999. Modeling the fate of pathogenic organisms in coastal waters of Oahu, Hawaii. J. Environ. Eng. 125 (5), 398–406. https://doi.org/10.1061/(asce)0733-9372(1999)125:5(398).
- DePaola, A., Capers, G.M., Alexander, D., 1994. Densities of *Vibrio vulnificus* in the intestines of fish from the U.S. Gulf Coast. Appl. Environ. Microbiol. 60 (3), 984–988. https://doi.org/10.1128/aem.60.3.984-988.1994.
- Fiedler, J.W., McManus, M.A., Tomlinson, M.S., De Carlo, E.H., Pawlak, G.R., Steward, G.F., Nigro, O.D., Timmerman, R.E., Drupp, P.S., Ostrander, C.E., 2014. Real-time observations of the February 2010 Chile and March 2011 Japan tsunamis recorded in Honolulu by the Pacific Islands Ocean Observing System. Oceanography 27 (2), 186–200. https://doi. org/10.5670/oceanog.2014.34.
- Froelich, B.A., Daines, D.A., 2020. In hot water: effects of climate change on Vibrio-human interactions. Environ. Microbiol. 22 (10), 4101–4111. https://doi.org/10.1111/1462-2920.14967.
- Ghosh, A., Bhadury, P., 2019. Exploring biogeographic patterns of bacterioplankton communities across global estuaries. MicrobiologyOpen 8 (5), 741. https://doi.org/10.1002/mbo3.741.
- Giambelluca, T.W., Chen, Q., Frazier, A.G., Price, J.P., Chen, Y.L., Chu, P.S., Eischeid, J.K., Delparte, D.M., 2013. Online rainfall atlas of hawai 'i. Bull. Am. Meteorol. Soc. 94 (3), 313–316. https://doi.org/10.1175/BAMS-D-11-00228.1.
- Givens, C.E., Bowers, J.C., Depaola, A., Hollibaugh, J.T., Jones, J.L., 2014. Occurrence and distribution of Vibrio vulnificus and Vibrio parahaemolyticus - potential roles for fish, oyster, sediment and water. Lett. Appl. Microbiol. 58 (6), 503–510. https://doi.org/10.1111/ lam.12226.
- Gordon, D.G., 1969. Examination of methods of particulate organic carbon analysis. Deep-Sea Res. Oceanogr. Abstr. 16 (6), 661–665. https://doi.org/10.1016/0011-7471(69)90066-7
- Grasshoff, K., Kremling, K., Ehrhardt, M., 1983. Methods of seawater analysis. Mar. Chem. 7 (1), 86–87. https://doi.org/10.1016/0304-4203(78)90045-2.
- Heng, S.P., Letchumanan, V., Deng, C.Y., Ab Mutalib, N.S., Khan, T.M., Chuah, L.H., Chan, K.G., Goh, B.H., Pusparajah, P., Lee, L.H., 2017. Vibrio vulnificus: an environmental and clinical burden. Front. Microbiol. 8, 997. https://doi.org/10.3389/fmicb.2017.00997.
- Holland, P.M., Abramson, R.D., Watson, R., Gelfand, D.H., 1991. Detection of specific polymerase chain reaction product by utilizing the 5′ → 3′ exonuclease activity of Thermus aquaticus DNA polymerase. Proc. Natl. Acad. Sci. U. S. A. 88 (16), 7276–7280. https://doi.org/10.1073/pnas.88.16.7276.
- Horseman, M.A., Surani, S., 2011. A comprehensive review of Vibrio vulnificus: an important cause of severe sepsis and skin and soft-tissue infection. Int. J. Infect. Dis. 15 (3), e157–e166. https://doi.org/10.1016/j.ijid.2010.11.003.
- Huang, K.C., Weng, H.H., Yang, T.Y., Chang, T.S., Huang, T.W., Lee, M.S., 2016. Distribution of fatal Vibrio vulnificus necrotizing skin and soft-tissue infections a systematic review and meta-analysis. Medicine 95 (5). https://doi.org/10.1097/MD.0000000000002627.
- Huehn, S., Eichhorn, C., Urmersbach, S., Breidenbach, J., Bechlars, S., Bier, N., Alter, T., Bartelt, E., Frank, C., Oberheitmann, B., Gunzer, F., Brennholt, N., Böer, S., Appel, B., Dieckmann, R., Strauch, E., 2014. Pathogenic vibrios in environmental, seafood and clinical sources in Germany. Int. J. Med. Microbiol. 304 (7), 843–850. https://doi.org/10.1016/j.ijmm.2014.07.010.
- IPCC, 2014. Climate change 2014: synthesis report. In: Core Writing Team, Pachauri, R.K., Meyer, L.A. (Eds.), Contribution of Working Groups I, II and III to the Fifth Assessment Report of the Intergovernmental Panel on Climate Change. IPCC, Geneva, Switzerland, p. 151.. https://www.ipcc.ch/site/assets/uploads/2018/05/SYR_AR5_FINAL_full_wcover.pdf.
- Jacobs, J.M., Rhodes, M., Brown, C.W., Hood, R.R., Leight, A., Long, W., Wood, R., 2014.
 Modeling and forecasting the distribution of Vibrio vulnificus in Chesapeake Bay.
 J. Appl. Microbiol. 117 (5), 1312–1327. https://doi.org/10.1111/jam.12624.
- Johnson, K.S., Coletti, L.J., 2002. In situ ultraviolet spectrophotometry for high resolution and long-term monitoring of nitrate, bromide and bisulfide in the ocean. Deep-Sea Res. I Oceanogr. Res. Pap. 49 (7), 1291–1305. https://doi.org/10.1016/S0967-0637(02) 00020-1
- Johnson, C.N., Flowers, A.R., Noriea, N.F., Zimmerman, A.M., Bowers, J.C., DePaola, A., Grimes, D.J., 2010. Relationships between environmental factors and pathogenic vibrios in the northern gulf of Mexico. Appl. Environ. Microbiol. 76 (21), 7076–7084. https:// doi.org/10.1128/AEM.00697-10.
- Johnson, A.E., Powell, B.S., Steward, G.F., 2013. Characterizing the effluence near waikiki, Hawaii with a coupled biophysical model. Cont. Shelf Res. 54, 1–13. https://doi.org/ 10.1016/j.csr.2012.12.007.
- Jones, M.K., Oliver, J.D., 2009. Vibrio vulnificus: disease and pathogenesis. Infect. Immun. 77 (5), 1723–1733. https://doi.org/10.1128/IAI.01046-08.
- Kan, J., Suzuki, M.T., Wang, K., Evans, S.E., Chen, F., 2007. High temporal but low spatial heterogeneity of bacterioplankton in the Chesapeake Bay. Appl. Environ. Microbiol. 73 (21), 6776–6789. https://doi.org/10.1128/AEM.00541-07.
- Kaspar, C.W., Tamplin, M.L., 1993. Effects of temperature and salinity on the survival of Vibrio vulnificus in seawater and shellfish. Appl. Environ. Microbiol. 59 (8), 2425–2429. https:// doi.org/10.1128/aem.59.8.2425-2429.1993.
- Kérouel, R., Aminot, A., 1997. Fluorometric determination of ammonia in sea and estuarine waters by direct segmented flow analysis. Mar. Chem. 57 (3–4), 265–275. https://doi. org/10.1016/S0304-4203(97)00040-6.

- Lipp, E.K., Rodriguez-Palacios, C., Rose, J.B., 2001. Occurrence and distribution of the human pathogen Vibrio vulnificus in a subtropical Gulf of Mexico estuary. The Ecology and Etiology of Newly Emerging Marine Diseases, pp. 165–173 https://doi.org/10.1007/978-94-017-3284-0 15.
- Martinez-Urtaza, J., Bowers, J.C., Trinanes, J., DePaola, A., 2010. Climate anomalies and the increasing risk of Vibrio parahaemolyticus and Vibrio vulnificus illnesses. Food Res. Int. 43 (7), 1780–1790. https://doi.org/10.1016/j.foodres.2010.04.001.
- Maugeri, T.L., Carbone, M., Fera, M.T., Gugliandolo, C., 2006. Detection and differentiation of Vibrio vulnificus in seawater and plankton of a coastal zone of the Mediterranean Sea. Res. Microbiol. 157 (2), 194–200. https://doi.org/10.1016/j.resmic.2005.06.007.
- McKinney, W., 2011. pandas: a foundational python library for data analysis and statistics. Retrieved fromPython for High Performance and Scientific Computing , pp. 1–9. https://www.dlr.de/sc/portaldata/15/resources/dokumente/pyhpc2011/submissions/pyhpc2011 submission 9.ndf.
- McManus, M.A., 2008. updated 2016. PacIOOS Nearshore Sensor 02 (NS02): Hawaii Yacht Club, Oahu, Hawaii. [1 October 2018 1 October 2019.]. Distributed by the Pacific Islands Ocean Observing System (PacIOOS) Accessed 16 December 2019 http://pacioos.org/metadata/NS02agg.html.
- Motes, M.L., DePaola, A., Cook, D.W., Veazey, J.E., Hunsucker, J.C., Garthright, W.E., Blodgett, R.J., Chirtel, S.J., 1998. Influence of water temperature and salinity on Vibrio vulnificus in northern gulf and Atlantic Coast oysters (Crassostrea virginica). Appl. Environ. Microbiol. 64 (4), 1459–1465. https://doi.org/10.1128/aem.64.4.1459-1465.1998.
- Muhling, B.A., Jacobs, J., Stock, C.A., Gaitan, C.F., Saba, V.S., 2017. Projections of the future occurrence, distribution, and seasonality of three vibrio species in the Chesapeake Bay under a high-emission climate change scenario. GeoHealth 1 (7), 278–296. https://doi. org/10.1002/2017GH000089.
- Murphy, J., Riley, J.P., 1962. A modified single solution method for the determination of phosphate in natural waters. Anal. Chim. Acta 27 (C), 31–36. https://doi.org/10.1016/ S0003-2670(00)88444-5.
- Nelson, N.B., Siegel, D.A., 2013. The global distribution and dynamics of chromophoric dissolved organic matter. Annu. Rev. Mar. Sci. 5, 447–476. https://doi.org/10.1146/annurey-marine-120710-100751.
- Nelson, C.E., Donahue, M.J., Dulaiova, H., Goldberg, S.J., La Valle, F.F., Lubarsky, K., Miyano, J., Richardson, C., Silbiger, N.J., Thomas, F.I.M., 2015. Fluorescent dissolved organic matter as a multivariate biogeochemical tracer of submarine groundwater discharge in coral reef ecosystems. Mar. Chem. 177, 232–243. https://doi.org/10.1016/j.marchem. 2015.06.026.
- Newton, A., Kendall, M., Vugia, D.J., Henao, O.L., Mahon, B.E., 2012. Increasing rates of vibriosis in the United States, 1996-2010: review of surveillance data from 2 systems. Clin. Infect. Dis. 54, 391–395. https://doi.org/10.1093/cid/cis243.
- Nigro, O.D., Steward, G.F., 2015. Differential specificity of selective culture media for enumeration of pathogenic vibrios: advantages and limitations of multi-plating methods. J. Microbiol. Methods 111, 24–30. https://doi.org/10.1016/j.mimet.2015.01.014.
- Nigro, O.D., James-Davis, L.I., De Carlo, E.H., Li, Y.H., Steward, G.F., 2022. Variable freshwater influences on the abundance of Vibrio vulnificus in a tropical urban estuary. Applied and Environmental Microbiology 88 (6). https://doi.org/10.1128/AEM.01884-21.
- Nuss, E., 2016. Predicting pathogenic bacteria concentrations with a coupled microbial-physical model. Retrieved fromProQuest Dissertations Publishing. https://www.soest.hawaii.edu/oceanography/masters/2016-Nuss.pdf.
- O'Neill, K.R., Jones, S.H., Grimes, D.J., 1992. Seasonal incidence of *Vibrio vulnificus* in the Great Bay estuary of New Hampshire and Maine. Appl. Environ. Microbiol. 58 (10), 3257–3262. https://doi.org/10.1128/aem.58.10.3257-3262.1992.
- Paz, S., Bisharat, N., Paz, E., Kidar, O., Cohen, D., 2007. Climate change and the emergence of Vibrio vulnificus disease in Israel. Environ. Res. 103 (3), 390–396. https://doi.org/10. 1016/j.envres.2006.07.002.
- Pfaffl, M.W., 2001. A new mathematical model for relative quantification in real-time RT– PCR. Nucleic Acids Res. 29 (9), E45. https://doi.org/10.1093/nar/29.9.e45.
- Pfeffer, C.S., Hite, M.F., Oliver, J.D., 2003. Ecology of Vibrio vulnificus in estuarine waters of eastern North Carolina. Appl. Environ. Microbiol. 69 (6), 3526–3531. https://doi.org/ 10.1128/AEM.69.6.3526-3531.2003.
- Python Core Team, 2015. Python: a dynamic, open source programming language. Python Software Foundation. https://www.python.org/.
- R Core team, 2019. R: a language and environment for statistical computing. URLR Foundation for Statistical Computing, Vienna, Austria. https://www.R-project.org/.

- Ralston, E.P., Kite-Powell, H., Beet, A., 2011. An estimate of the cost of acute health effects from food- and water-borne marine pathogens and toxins in the USA. J. Water Health 9 (4), 680–694. https://doi.org/10.2166/wh.2011.157.
- Randa, M.A., Polz, M.F., Lim, E., 2004. Effects of temperature and salinity on *Vibrio vulnificus* population dynamics as assessed by quantitative PCR. Appl. Environ. Microbiol. 70 (9), 5469–5476. https://doi.org/10.1128/AEM.70.9.5469-5476.2004.
- Rivera, S., Lugo, T., Hazen, T.C., 1989. Autecology of Vibrio vulnificus and Vibrio parahaemolyticus in tropical waters. Water Res. 23 (7), 923–931. https://doi.org/10.1016/0043-1354(89)90018-3.
- Ruhala, S.S., Zarnetske, J.P., 2017. Using in-situ optical sensors to study dissolved organic carbon dynamics of streams and watersheds: a review. Sci. Total Environ. 575, 713–723. https://doi.org/10.1016/j.scitotenv.2016.09.113.
- Sharp, J.H., 1974. Improved analysis for "particulate" organic carbon and nitrogen from seawater. Limnol. Oceanogr. 19, 984–989. https://doi.org/10.4319/lo.1974.19.6.0984.
- Shiller, A.M., 1996. The effect of recycling traps and upwelling on estuarine chemical flux estimates. Geochim. Cosmochim. Acta 60 (17), 3177–3185. https://doi.org/10.1016/0016-7037(96)00159-7.
- Smith, R.C., Baker, K.S., Dustan, P., 1981. Fluorometric techniques for the measurement of oceanic chlorophyll in the support of remote sensing. UC San Diego: Library – Scripps Digital Collection. https://escholarship.org/uc/item/4k51f7p0.
- Strom, M.S., Paranjpye, R.N., 2000. Epidemiology and pathogenesis of Vibrio vulnificus. Microbes Infect. 2, 177–188. https://doi.org/10.1016/S1286-4579(00)00270-7.
- Tamplin, M., Rodrick, G.E., Blake, N.J., Cuba, T., 1982. Isolation and characterization of Vibrio vulnificus from two Florida estuaries. Appl. Environ. Microbiol. 44 (6), 1466–1470. https://doi.org/10.1128/aem.44.6.1466-1470.1982.
- Turner, J.W., Good, B., Cole, D., Lipp, E.K., 2009. Plankton composition and environmental factors contribute to vibrio seasonality. ISME J. 3 (9), 1082–1092. https://doi.org/10. 1038/ismei.2009.50.
- Vezzulli, L., Brettar, I., Pezzati, E., Reid, P.C., Colwell, R.R., Höfle, M.G., Pruzzo, C., 2012. Long-term effects of ocean warming on the prokaryotic community: evidence from the vibrios. ISME J. 6 (1), 21–30. https://doi.org/10.1038/ismej.2011.89.
- Vezzulli, L., Colwell, R.R., Pruzzo, C., 2013. Ocean warming and spread of pathogenic vibrios in the aquatic environment. Microb. Ecol. 65 (4), 817–825. https://doi.org/10.1007/ s00248-012-0163-2.
- Vezzulli, L., Grande, C., Reid, P.C., Hélaouët, P., Edwards, M., Höfle, M.G., Brettar, I., Colwell, R.R., Pruzzo, C., 2016. Climate influence on Vibrio and associated human diseases during the past half-century in the coastal North Atlantic. Proc. Natl. Acad. Sci. U. S. A. 113 (34). https://doi.org/10.1073/pnas.1609157113 E5062–E5071.
- Viau, E.J., Goodwin, K.D., Yamahara, K.M., Layton, B.A., Sassoubre, L.M., Burns, S.L., Tong, H., Wong, S.H.C., Lu, Y., Boehm, A.B., 2011. Bacterial pathogens in Hawaiian coastal streams—associations with fecal indicators, land cover, and water quality. Water Res., 3279–3290 https://doi.org/10.1016/j.watres.2011.03.033.
- Vithanage, G., 2011. The prevalence and public health significance of human pathogenic vibrio species (V. cholerae, V. vulnificus, V. parahaemolyticus, V. alginolyticus) in Hawai'i's diverse tropical coastal water environments. Doctoral Dissertation, University of Hawaii at Manoa. http://hdl.handle.net/10125/101779. (Accessed 8 March 2022).
- Wetz, J.J., Blackwood, A.D., Fries, J.S., Williams, Z.F., Noble, R.T., 2013. Quantification of Vibrio vulnificus in an estuarine environment: a multi-year analysis using QPCR. Estuar. Coasts 37 (2), 421–435. https://doi.org/10.1007/S12237-013-9682-4.
- Wright, A.C., Hill, R.T., Johnson, J.A., Roghman, M.C., Colwell, R.R., Morris, J.G., 1996. Distribution of Vibrio vulnificus in the Chesapeake Bay. Appl. Environ. Microbiol. 62 (2), 717–724. https://doi.org/10.1128/aem.62.2.717-724.1996.
- Zhang, C., Wang, Dr.Y., Lauer, A., Hamilton, K., 2012. Configuration and evaluation of the WRF model for the study of hawaiian regional climate. Mon. Weather Rev. 140 (10), 3259–3277. https://doi.org/10.1175/MWR-D-11-00260.1.
- Zhang, C., Wang, Y., Hamilton, K., Lauer, A., 2016a. Dynamical downscaling of the climate for the hawaiian islands. Part I: present day. J. Clim. 29 (8), 3027–3048. https://doi.org/10. 1175/JCLI-D-15-0432.1.
- Zhang, C., Wang, Y., Hamilton, K., Lauer, A., 2016b. Dynamical downscaling of the climate for the hawaiian islands. Part II: projection for the late twenty-first century. J. Clim. 29 (23), 8333–8354. https://doi.org/10.1175/JCLI-D-16-0038.1.